AGU PUBLICATIONS

Journal of Advances in Modeling Earth Systems

RESEARCH ARTICLE

10.1002/2015MS000504

Key Points:
- Soil/snow affect permafrost area, degradation much stronger than climate/land-cover differences
- Strongest role of deep soils on permafrost area, degradation but low impact in root zone states
- Energy/water fluxes are impacted more by climate/land-cover differences than soil/snow changes

Supporting Information:
- Supporting Information S1

Correspondence to:
R. Barman,
account1.rahul@gmail.com

Citation:
Barman, R., and A. K. Jain (2016), Comparison of effects of cold-region soil/snow processes and the uncertainties from model forcing data on permafrost physical characteristics, *J. Adv. Model. Earth Syst.*, *8*, doi:10.1002/2015MS000504.

Received 25 JUN 2015
Accepted 23 JAN 2016
Accepted article online 28 JAN 2016

Comparison of effects of cold-region soil/snow processes and the uncertainties from model forcing data on permafrost physical characteristics

Rahul Barman[1] and Atul K. Jain[1]

[1]Department of Atmospheric Sciences, University of Illinois, Urbana, Illinois, USA

Abstract We used a land surface model to (1) evaluate the influence of recent improvements in modeling cold-region soil/snow physics on near-surface permafrost physical characteristics (within 0–3 m soil column) in the northern high latitudes (NHL) and (2) compare them with uncertainties from climate and land-cover data sets. Specifically, four soil/snow processes are investigated: deep soil energetics, soil organic carbon (SOC) effects on soil properties, wind compaction of snow, and depth hoar formation. In the model, together they increased the contemporary NHL permafrost area by 9.2×10^6 km^2 (from 2.9 to 12.3—without and with these processes, respectively) and reduced historical degradation rates. In comparison, permafrost area using different climate data sets (with annual air temperature difference of ~0.5°C) differed by up to 2.3×10^6 km^2, with minimal contribution of up to 0.7×10^6 km^2 from substantial land-cover differences. Individually, the strongest role in permafrost increase was from deep soil energetics, followed by contributions from SOC and wind compaction, while depth hoar decreased permafrost. The respective contribution on 0–3 m permafrost stability also followed a similar pattern. However, soil temperature and moisture within vegetation root zone (~0–1 m), which strongly influence soil biogeochemistry, were only affected by the latter three processes. The ecosystem energy and water fluxes were impacted the least due to these soil/snow processes. While it is evident that simulated permafrost physical characteristics benefit from detailed treatment of cold-region biogeophysical processes, we argue that these should also lead to integrated improvements in modeling of biogeochemistry.

1. Introduction

With the NHL regions warming continually, it is increasingly important to quantify the thermal state of current permafrost as well as its future degradation. While there is a consensus that near-surface permafrost (hereon simply referred to as permafrost) area will continue to decrease with climate warming, the rate of degradation produced by modeling studies remain highly divergent [*Eliseev et al.*, 2009; *Euskirchen et al.*, 2006; *Koven et al.*, 2013; *Lawrence et al.*, 2008; *Marchenko et al.*, 2008; *Saito et al.*, 2007; *Schaefer et al.*, 2011]. Changes in permafrost can impact regional terrestrial energetics, hydrology, and ecology; consequently, large-scale permafrost thaw is expected to mobilize the soil carbon and tremendously impact global climate [*Grosse et al.*, 2011; *McGuire et al.*, 2006; *Schuur et al.*, 2012, 2015]. However, in marked contrast to their recognized importance, our understanding of permafrost and observations of high-latitude soil/snow processes remain sparse [*ACIA*, 2004; *Boike et al.*, 2012].

An underlying difficulty arises in modeling the contemporary Northern Hemisphere permafrost area itself, as evident from the diagnosed range of $1.5–27.3 \times 10^6$ km^2 (during 2005) across the recent Coupled Model Intercomparison Project (CMIP5) earth system models (ESMs) [*Koven et al.*, 2013]. Subsequent model diagnoses have attributed several deficiencies in model structure and parameterizations, mostly related to representation of soil and snow thermal processes such as: (1) thermal coupling between deep and shallow soils, (2) impact of soil properties due to organic content, (3) representation of snow physics and insulation processes, (4) inclusion/exclusion of energy transfer from phase change, (5) interactions between soil energetics and hydrology, etc. [*Koven et al.*, 2013; *Slater and Lawrence*, 2013]. In these studies, the authors noted that the majority of current models do not represent many of these processes, causing a wide range in simulated permafrost area and degradation rate. In addition, the climate forcing (meteorology) can also influence the permafrost through the modification of energy/water exchange between the atmosphere and the soil

surface. Across currently available ESMs, the computed meteorology can be highly divergent. Similarly, in simulations using land surface models (LSMs), the meteorology from one of many available reanalyses can also be sufficiently different [*Dee et al*., 2015], which can cause divergent permafrost estimates. A previous study [*Slater and Lawrence*, 2013] investigated the role of climate biases on the diagnosed permafrost in CMIP5 ESMs, by using diagnostic indices to isolate the contributions of model-simulated climate on permafrost, from those due to model structure. Their analysis shows that biased climate can significantly degrade permafrost predictions. However, given their use of indirect and simplified indices for this analysis, a direct estimation of permafrost sensitivity to meteorology/climate (such as in a LSM framework) remains necessary. Furthermore, the modeling of permafrost physical characteristics in the NHL is most likely to suffer from considerable differences in current land-cover data sets [*Meiyappan and Jain*, 2012]. The extent of impacts from such uncertainties in tandem with model (soil/snow) structural differences has not been quantified in existing literature.

Here we performed such an integrated analysis using a LSM to (1) study the sensitivity of permafrost physical characteristics to specific improvements in cold-region soil/snow thermal processes and (2) compare the importance of such changes in model structure and parameterizations with modeling uncertainties from climate and land-cover data sets. Specifically, model structural improvements are represented using two soil and two snow processes that are prevalent in the NHL environment: (1) energy exchange between shallow and deep soils, by representing soils up to ~50 m [*Lawrence et al*., 2008], (2) effect of soil organic carbon (SOC) on thermal/hydrological properties [*Lawrence and Slater*, 2008], (3) wind compaction of snow depth (and density) [*Anderson*, 1976; *Schaefer et al*., 2009], and (4) depth hoar formation in snow [*Anderson*, 1976; *Schaefer et al*., 2009; *Zhang et al*., 1996]. A conceptual diagram of these processes and how they interact with permafrost physical characteristics is shown in Figure 1. Extending from previous studies [*Chadburn et al*., 2015; *Dankers et al*., 2011; *Lawrence et al*., 2008; *Schaefer et al*., 2009], a key goal of the current study was to quantify the *individual* contribution of these soil/snow processes on multiple variables: permafrost extent, area, degradation, soil thermal, and hydrological states for the entire NHL. The responses from these soil/snow improvements are then contrasted with driver-induced uncertainties from two reanalysis (climate) data sets and two land-cover data sets cover within the single unified model domain. Finally, we also investigated the sensitivity of permafrost area to a seemingly standard factor in model diagnosis of permafrost—the choice of threshold soil temperature (by default chosen as mean monthly temperature of 0°C), the results of which yield interesting insights. We discuss the implications of our results in the context of divergent permafrost area estimates from multimodel intercomparison projects, and soil biogeochemical calculations.

2. Methods

2.1. Model

We used the Integrated Science Assessment Model (ISAM), a LSM with coupled biogeophysical [*Barman et al*., 2014a, 2014b] and biogeochemical processes [*El-Masri et al*., 2013; *Yang et al*., 2009]. Energy, water, and momentum fluxes are updated hourly, with a spatial resolution of 0.5° × 0.5°. Each model grid is subdivided into multiple vegetation types, bare soil, and land ice [*Meiyappan and Jain*, 2012]. Besides the four soil/snow processes already introduced (energy exchange between shallow and deep soil; effects of SOC on soil properties; wind compaction of snow; depth hoar formation), the model also incorporates the following processes among others: multilayer snow physics using dynamic snow layers over the soil column; snow compaction due to weight, thermal aging, and melting; latent heat from phase change; and impact of supercooled water on hydraulic conductivity. Key equations and description of all these processes are available in supporting information Text S1. The processes of wind compaction of snow and depth hoar formation are parameterized using snow classification data (supporting information Figure S1) [*Sturm et al*., 1995]. For calculation of soil properties, SOC in observationally affected permafrost area (from the International Permafrost Association: IPA [*Brown et al*., 1997]) is initialized from the Northern Circumpolar Soil Carbon Database (NCSCD) [*Hugelius et al*., 2014; *Tarnocai et al*., 2009]. At other grid cells, the Harmonized World Soil Database (HWSD) [*FAO/IIASA/ISRIC/ISS-CAS/JRC*, 2012] is used.

2.2. Climate Data Sets

We used two reanalysis data sets to simulate the differences due to climate on permafrost: (1) the CRUNCEP [*Viovy and Ciais*, 2011; *Wei et al*., 2013] available up to 2010 and (2) the NCEP/NCAR [*Qian et al*., 2006] available

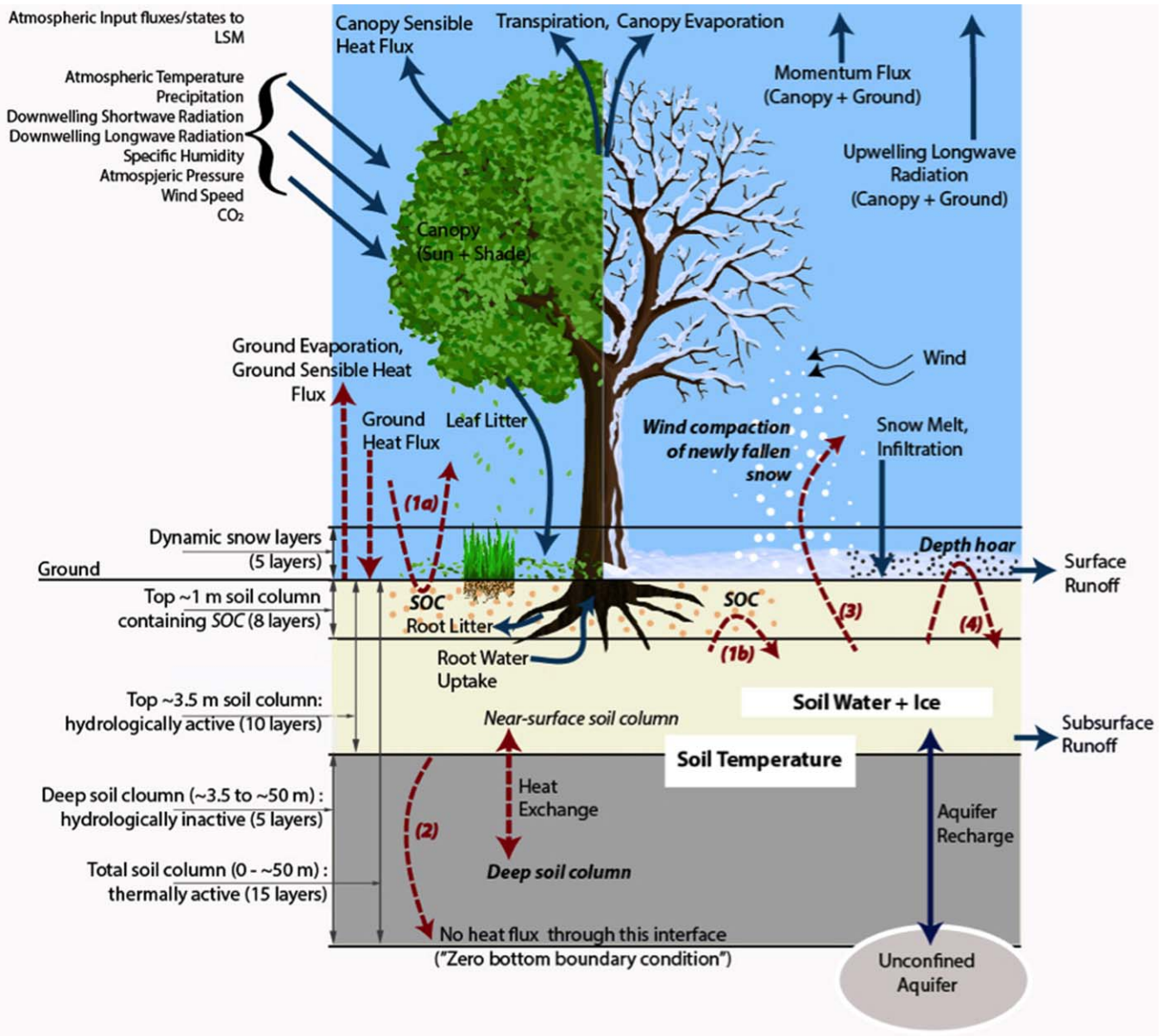

Figure 1. Conceptual diagram of model biogeophysics, focusing on the four key cold-region soil/snow processes used in this study. Specifically, they are effects of *SOC* on thermal and hydrological properties, incorporation of a deep soil column, wind compaction of snow, and depth hoar formation in snow. Thermal processes that are directly affected by these are shown with red dotted arrows labeled as: (1a) SOC-induced soil cooling in summer due to the increased insulation to the incoming ground heat flux; (1b) SOC-induced soil warming in winter by the reduction of net outgoing ground heat flux; (2) heat exchange between shallow and deep soils by shifting the "zero" bottom boundary condition to ~50 m; (3) wind-speed-driven snow compaction, increasing the winter snow thermal conductivity and cooling soils by increasing the outgoing ground heat flux; (4) reduction of snow thermal conductivity due to the formation of insulating depth hoar crystals in winter, thereby warming the soils. There are other thermal/hydrological interactions among these processes, the effects of which are simulated by the model.

up to 2004 (subsequently referred as NCEP). From these data sets, the meteorological fields utilized into the model are air temperature, precipitation, short-wave (solar) radiation, long-wave radiation, humidity, and atmospheric pressure. There are substantial spatial differences in these fields between the two reanalyses (supporting information Figure S2), which can result in significantly large differences in terrestrial ecosystem fluxes (latent heat, sensible heat, runoff, and carbon fluxes) using land surface models [*Barman et al.*, 2014a, 2014b]. Notably, averaged over the NHL region (45°N–90°N) these reanalyses have approximately equal trends in climate warming, but atmospheric temperature in the former is ~0.5°C cooler (supporting information Figure S3).

2.3. Land-Cover Data Sets

To represent land-cover uncertainty on permafrost, we used two data sets. Both are based on land use information (crop and pasture) from HYDE [*Klein Goldewijk et al.*, 2011] but vary in the method of

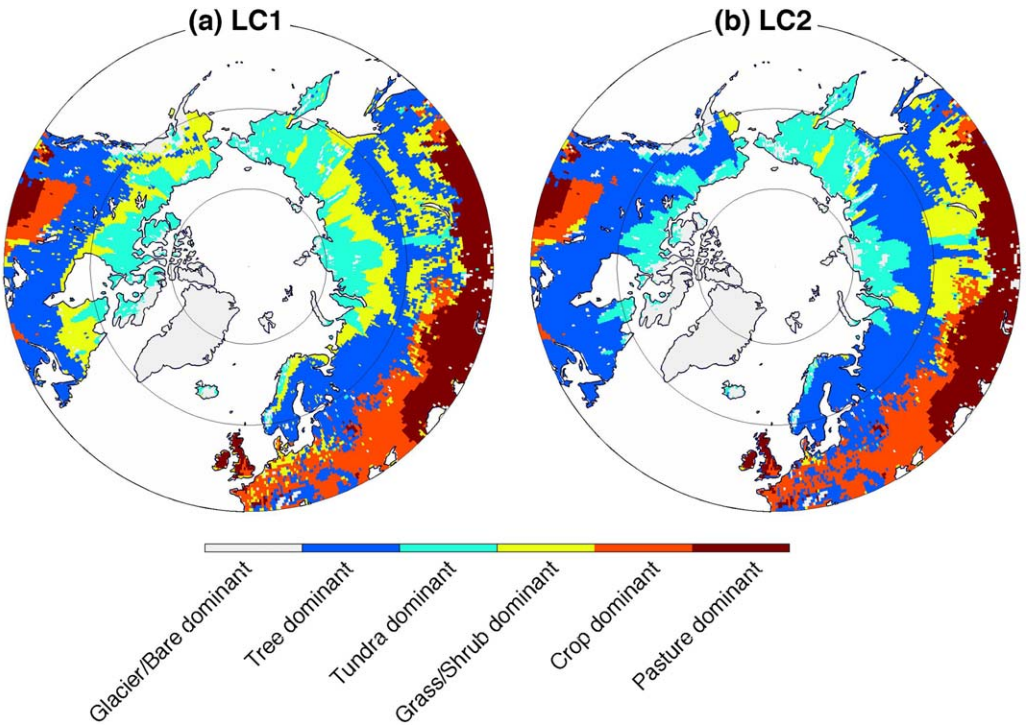

Figure 2. Maps of dominant vegetation types in two different land-cover data sets used in this study: (a) LC1 and (b) LC2, poleward of 45°N and shown for the year 2005. Though only the dominant vegetation is shown, each 0.5° × 0.5° grid cell may contain multiple vegetation types and can vary annually due to land use change.

reconstruction for forest area [*Meiyappan and Jain*, 2012]. Here we refer to them as (1) LC1 based on satellite calibration of forest cover and (2) LC2 without satellite calibration (Figure 2). Each 0.5° × 0.5° grid cell (current model resolution) may contain multiple plant functional types (PFTs): temperate and boreal trees (each of evergreen and deciduous types), tundra, C_3/C_4 grass, shrubs, crops, pasture, bare soil, and glacier. Aggregated poleward of 45°N, the LC2 data set contains ~3.4×10^6 km^2 higher boreal tree area than LC1, compensated by lower natural herbaceous vegetation (grass, shrubs, tundra, etc.) [*Meiyappan and Jain*, 2012]. In both data sets, the land-cover changes annually due to land use change or other human activities and disturbances.

2.4. Experimental Setup

Focusing on the NHL region poleward of 45°N, we carried out a series of modeling experiments by varying the (1) representation of soil/snow physics (*MODEL*) in the model: four processes, (2) climate data sets (*CLIMATE*): CRUNCEP and NCEP, and (3) land-cover data sets (*LC*): LC1 and LC2. The CRUNCEP and the LC1 are used as baseline data sets. A description of the simulations performed is summarized in Table 1. We classified *MODEL* physics to *New*, *Old*, and *Interm* (intermediate). *New* includes all the four soil/snow processes (i.e., deep soils, SOC, wind compaction of snow, and depth hoar), *Old* excludes all these processes from *New*, and four *Interm* versions exclude one process from *New* at a time. First, to quantify the impacts of the soil/snow processes, we performed one simulation each for these six different realizations with the CRUNCEP reanalysis and LC1 land-cover data. These are labeled as *NEW*, *OLD*, *NEW-NO-DH*, *NEW-NO-DS*, *NEW-SOC*, and *NEW-NO-WIND* (first six setups in Table 1). Second, to assess driver-induced uncertainties, we tested a different combination of climate data set (NCEP) and land-cover data set (LC2) in *New* and *Old* soil/snow physics versions. Along with the first two simulations (*NEW* and *OLD*), these result in six additional simulations, labeled as: $NEW_{CRUNCEP\text{-}LC2}$, $OLD_{CRUNCEP\text{-}LC2}$, $NEW_{NCEP\text{-}LC1}$, $OLD_{NCEP\text{-}LC1}$, $NEW_{NCEP\text{-}LC2}$, and $OLD_{NCEP\text{-}LC2}$ (last six setups in Table 1).

We spun-up all simulations for ~250 years using respective meteorology from 1979 to 2004 (for NCEP) and 1979 to 2010 (for CRUNCEP). The 250 years were achieved by cycling through the available 26 years (for NCEP) and 32 years (for CRUNCEP). We did not perform any detrending on any meteorological field. The

Table 1. List of Model Experiments and Corresponding Permafrost Area (PA)[a]

	MODEL			CLIMATE		LC		
Experiment	New	Old	Interm	CRUNCEP	NCEP	LC1	LC2	PA 2000–2004 ($\times 10^6$ km^2)
NEW	✓			✓		✓		12.3
OLD		✓		✓		✓		2.9
NEW-NO-DH			✓	✓		✓		13.0
NEW-NO-DS			✓	✓		✓		8.7
NEW-NO-SOC			✓	✓		✓		9.6
NEW-NO-WIND			✓	✓		✓		10.3
$NEW_{CRUNCEP-LC2}$	✓			✓			✓	12.1
$OLD_{CRUNCEP-LC2}$		✓		✓			✓	3.1
$NEW_{NCEP-LC1}$	✓				✓	✓		10.5
$OLD_{NCEP-LC1}$		✓			✓	✓		2.6
$NEW_{NCEP-LC2}$	✓				✓		✓	9.9
$OLD_{NCEP-LC2}$		✓			✓		✓	2.7

[a]Soil/snow physics (*MODEL*) is classified as *New*, *Old*, and *Interm* (intermediate). Each *Interm* version was created by excluding one process from *NEW* at a time, as indicated by suffix: (1) *NO-DH*: no depth hoar, (2) *NO-DS*: no deep soil, (3) *NO-SOC*: no SOC, and (4) *NO-WIND*: no wind compaction of snow. *Old* was created by excluding all the aforementioned processes from *New*. For different simulations, the choice of meteorology (*CLIMATE*) was between the CRUNCEP and the NCEP, and the choice land-cover data set (*LC*) was between the LC1 and the LC2. Unless otherwise specified through the subscript, a simulation (i.e., the first six simulations) was driven using the CRUNCEP and the LC1.

data for atmospheric CO_2 concentration and land-cover were also varied annually based on transient conditions. Note that the model estimated permafrost using the current spin-up approach is not theoretically comparable to the real-world permafrost, which be a result of continual changes in climate, and other anthropogenically affected forcings (e.g., since the industrial revolution). Nonetheless, the characteristically short climate memory of 0–3 m thermal and hydrological variables makes the adopted approach practically useful. In the model, the ~50 m soil temperatures respond very slowly to the transient climate forcing, needing ~250–400 years of model spin-up time. This time scale can be lowered by using a partially spun-up, globally gridded soil temperature data (e.g., from previous model simulations) to initialize the current simulations uniformly. We used this approach to limit the spin-up time to 250 years for individual simulations. After the deep soils are spun-up, the 0–3 m soils spin-up much faster. Specifically in our simulations, ~5 years in the beginning of each perturbation cycle (from 1979 onward) were sufficient for the soil temperatures therein to shift to the new quasi steady state equilibrium with the transient climate. Therefore, in this study, we calculated the near-surface permafrost from 1985 onward, which eliminates the initial influence from repetitive model spin-up, and to a large extent accounts for limitations of the spin-up method. Consequently in our results, any change in permafrost area from 1985 onward would be due to external forcings, and not due to residual drifts from model spin-up.

Finally, here we reinstate that this paper diagnoses only the near-surface component of the permafrost, which is within the 0–3 m soil column. Specifically for a model grid cell, if the monthly averaged soil temperatures in any of the 0–3 m layers remain below 0°C for at least 24 months, we classify it as permafrost. This approach has been used in a previous CMIP5 study [*Koven et al.*, 2013]. Based on the definition of permafrost, glaciated areas were excluded.

3. Results and Discussion

3.1. Impact of the Cold-Region Soil/Snow Processes

3.1.1. Permafrost Area

Simulations using *NEW*, *OLD*, and four *Interm* versions show that there is a large variation in permafrost area based on cold-region soil/snow physics (Table 1 and Figure 3a). In *NEW*, the permafrost area contained between 45°N and 90°N is ~12.3 $\times$ 10^6 km^2 (averaged during 2000–2004), which compares favorably with corresponding observational estimates of 12.6–13.9 $\times$ 10^6 km^2 for continuous (90–100% coverage) and discontinuous (50–90% coverage) permafrost area [*Brown et al.*, 1997; *Zhang et al.*, 1999]. In contrast, there is a strong low bias in *OLD* (excluding all soil/snow improvements from *NEW*), which contain only 2.9 $\times$ 10^6 km^2 of permafrost area. Such estimates from *OLD* are similar to the lower limit of ~1.5–27.3 $\times$ 10^6 km^2 of permafrost area (diagnosed for 0°N–90°N) from the CMIP5 models [*Koven et al.*, 2013]. These findings strengthen the conclusion of previous studies that exclude the specific soil/snow processes (as investigated in this

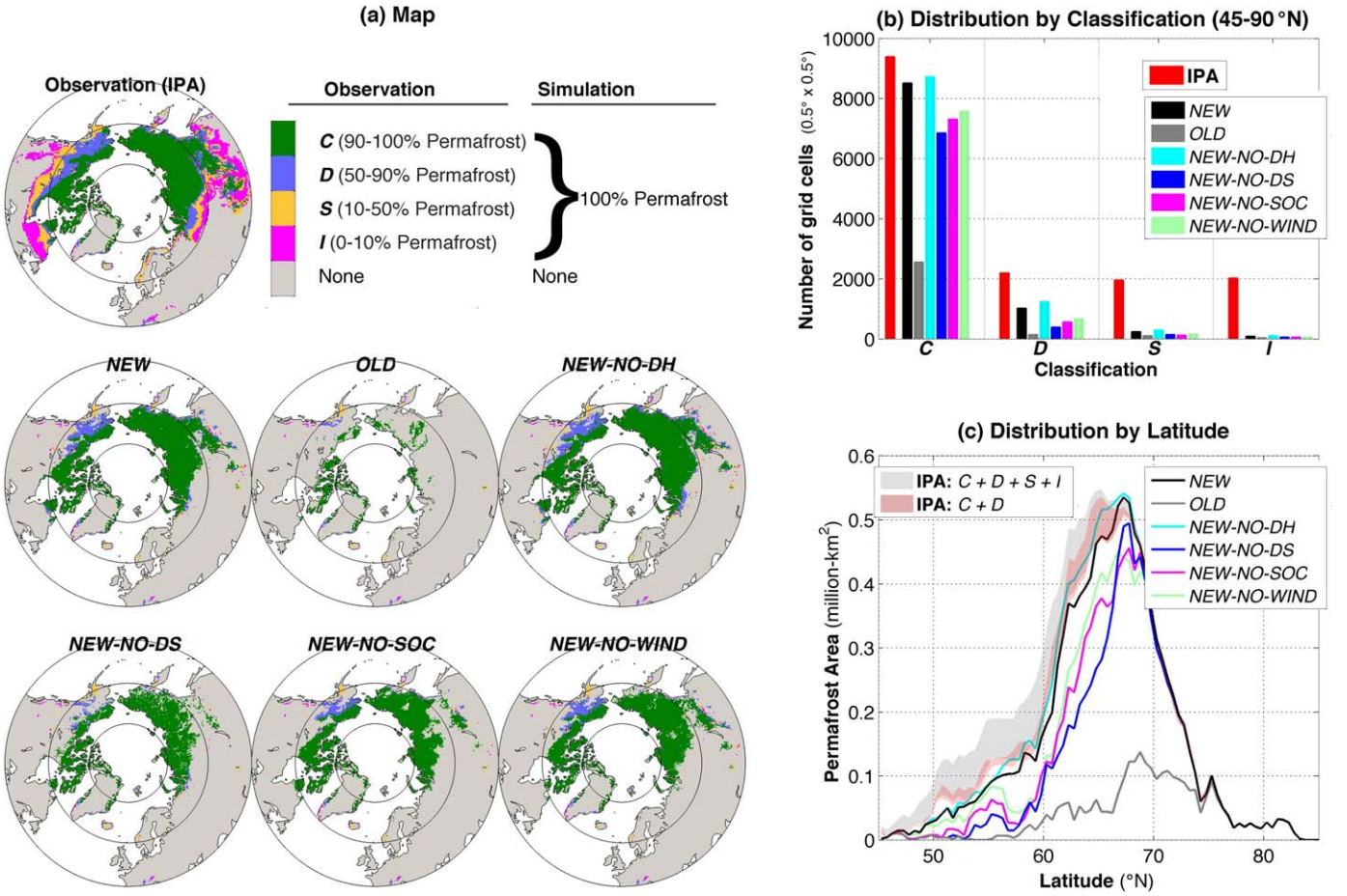

Figure 3. (a) Map of permafrost area (poleward of 45°N) by latitude in observations (International Permafrost Association, IPA) and simulations: *NEW*, *OLD*, and four *Interm* versions (*NEW-NO-DH*, *NEW-NO-DS*, *NEW-NO-SOC*, and *NEW-NO-WIND*). In observations, different permafrost classifications based on % grid cell coverage are continuous (*C*): 90–100%, discontinuous (*D*): 50–90%, sporadic (*S*): 10–50%, and isolated (*I*): 0–10%. In simulations, a grid cell is either 100% permafrost or no permafrost. For gridcells that are diagnosed as permafrost (i.e., 100% coverage) in respective simulations, the colors illustrate the observed pemafrost type therein. (b) Number of 0.5° × 0.5° grid cells within each classification in observations, and subset of respective grid cells diagnosed as permafrost in simulations. (c) Distribution of permafrost area by latitude. The range of observated permafrost area shown in shading was derived by weighting fractional coverage of different permafrost classifications. All the simulated results are using averaged output during 2000–2004.

study) and hence may potentially explain several model structure/parameterization related causes of very low permafrost diagnosed from some of the CMIP5 models.

We compared the model with observations by permafrost classification types (Figure 3b). It is evident that even though *NEW* is able to simulate permafrost in the grid cells classified as continuous (90–100% coverage) and discontinuous (50–90% coverage) permafrost in observations, it is mostly unable to diagnose permafrost in the sporadic (10–50% coverage) and isolated (0–10% coverage) regions. In the current model, there are no subgrid-scale processes that are required to capture sporadic and isolated classes, and permafrost in a grid cell is a Boolean characteristic, i.e., either a model grid cell there is completely covered in permafrost (100% coverage) or there is no permafrost in it (0% coverage). Therefore, the lack of these permafrost types in the model can be justified for the "right reasons." Therefore, current LSMs that do not contain subgrid-scale parameterizations for sporadic/isolated classes, and yet diagnose large-scale permafrost in these areas, would have cold soil temperature biases.

In comparison to *NEW*, there is a reduction of permafrost area in *OLD* across northern latitudes up to ~75°N, above which the soils are cold enough to be classified as permafrost regardless of the new modeling differences (Figure 3c). The individual *Interm* versions can explain large differences in simulated permafrost, mostly between 50°N and 70°N, above which exclusion of one of the four soil/snow processes at a time from *NEW* do not sufficiently affect the near-surface permafrost. Individually, the largest decrease in modeled permafrost area occurs with the exclusion of deep soils from the revised model (3.4×10^6 km^2)

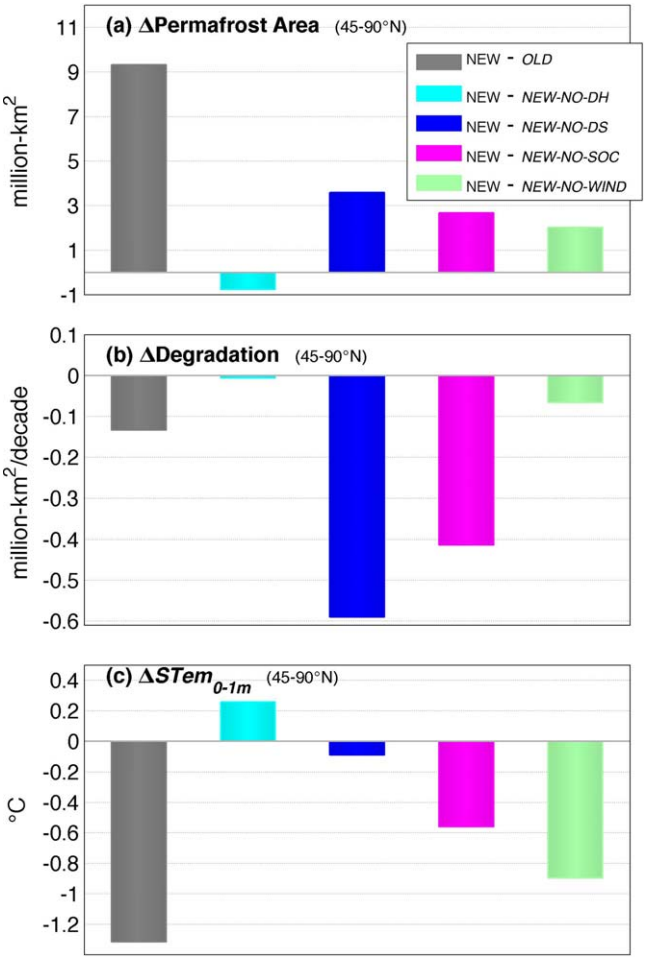

Figure 4. Simulated differences (Δ) in key permafrost physical characteristics in *OLD* and four *Interm* simulations with respect to *NEW*: in mean annual (a) permafrost area (averaged during 2000–2004), (b) degradation rate (from 1985 to 2010), and (c) soil temperature in 0–1 m depth ($STem_{0-1m}$, averaged during 2000–2004).

(Figure 4a). Similar experiments by excluding soil organic effects and wind compaction of snow, one at a time, also reduced the permafrost area by 2.4 and 1.8 $\times$ 10^6 km^2, respectively. These indicate that inclusion of these three processes have net cooling impacts in the top $\sim$3 m soil column (based on which the near-surface permafrost is diagnosed), consistent with previous studies [*Lawrence et al.*, 2008; *Schaefer et al.*, 2009]. Mechanistically, deep soils increase permafrost stability by shifting the "zero bottom boundary condition" (i.e., zero heat exchange) below the deepest soil layer (>40 m), which lowers the thermal gradient, as well as the ground heat flux into the soil in summer and out of soil in winter. Effectively, this provides a larger reservoir for soil heat storage, which mitigates the fluctuation of temperature variability in the near-surface soil column, and decreases the net soil temperatures in the near-surface soil column from annual to decadal time scales. SOC also has a net cooling impact of mean annual soil temperatures that increases the permafrost area. In the summer, SOC acts as an insulator to the heat from incoming radiation—thereby cooling the soil; in the winter, the same insulating properties of SOC mitigate the heat flow out of the soil column—thereby warming the soil. Note that the effect of SOC in winter is probably less critical because there is the insulating layer of snow above it. The net annual impact from these opposing processes is still a substantial cooling [*Lawrence and Slater*, 2008]. Finally, in winter, the wind compaction of snow reduces the otherwise strong thermal insulation from snow. This facilitates larger heat flows out of the soil column to atmosphere, which contribute in cooling the mean annual soil temperatures. Therefore, above 70°N, in *NEW-NO-DS* where deep soils are absent, combined cooling from SOC in summer and wind compaction of snow still sufficiently cool the soils to be classified as permafrost. In *NEW-NO-SOC*, deep soils and wind impacts keep the permafrost to comparable amounts as in *NEW-NO-DS*. Finally, the inclusion of depth hoar parameterization resulted in reduction of permafrost area ($\sim$0.8 $\times$ 10^6 km^2). This is because when the depth hoar parameterization is present, there is an increase in winter insulation of snow, which consequently warms winter/spring soil temperatures [*Schaefer et al.*, 2009; *Sellers et al.*, 1996].

While the formulation of deep soils affects all grid cells, the SOC impacts vary geographically depending on how much SOC is present within the respective grid cell. Generally, the entire NHL permafrost area is rich in SOC, and therefore the SOC effect in this area is stronger than that in nonpermafrost areas. Wind compaction of snow, and depth hoar formation are also regionally varying and depend on wind speed, snow depth, categorization of snow, etc. (as discussed previously). In the model, wind compaction of snow (Figure 5) is parameterized for the tundra and the prairie snow class regions (supporting information Figure S1), which are characterized by strong wind speeds (supporting information Figure S4). Specially for the tundra, snow compaction by wind appears to be as large as $\sim$0.15 m, which are very substantial given that much of the

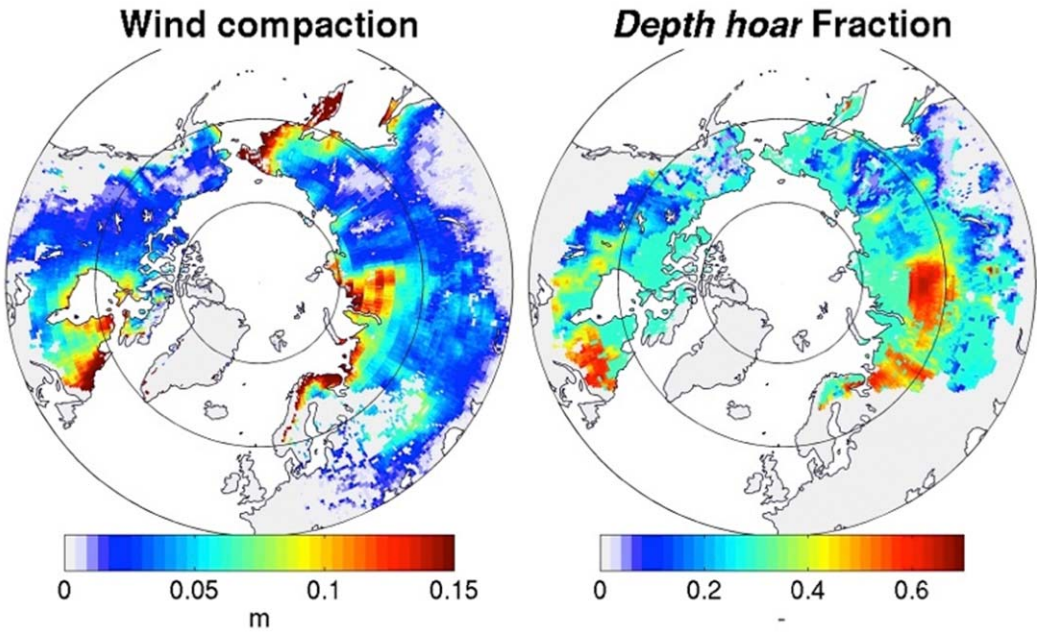

Figure 5. (left) Wind compaction of snow and (right) depth hoar formation during winter months of December-January-February (DJF). Wind compaction of snow depth is shown in meters, and depth hoar amount is shown as a fraction (0–1) of total snow depth.

Arctic have *peak* snow depths of less than 0.5 m [*Brown and Brasnett*, 2010]. The scheme for depth hoar formation is active in the tundra and the taiga snow class regions. Typically, depth hoar (Figure 5) is confined to regions with greatest snow depths, because depth hoar formation only occurs above a certain snow depth [*Schaefer et al*., 2009]. Nonetheless, because such schemes are available (and dominant) in certain snow class types, it can result in abrupt transitions, such as in depth hoar fraction just southeast of the Ob river delta. Note that because wind compaction of snow and depth hoar formation depends on snow amount, wind speed, etc., where their role will be significant in future will most likely be dependent on geographical pattern of climate change, land-cover change, as well as on dynamic changes of snow classes itself.

3.1.2. Permafrost Degradation (1985–2010)

Along with the higher permafrost area, the permafrost degradation in *NEW* also appears to be largely reduced, by as low as 0.15×10^6 km^2/decade during 1985–2010 (Figure 4b). Note that there is interannual variability in permafrost area time series (Figure 6a) as evident from the sawtooth pattern therein. This is primarily due to the interannual variability in air temperature itself. Assessing the individual contributions relative to *NEW* shows that largest increases in permafrost degradation occur when soil physical improvements are excluded from the model (i.e., deep soil and SOC impacts), with lower impacts from snow-related changes (depth hoar formation and wind compaction of snow). This is corroborated in Figure 6b, which shows that removal of deep soils (*NEW-NO-DS*) or SOC (*NEW-NO-SOC*) lead to the largest amplitudes of interannual fluctuations in permafrost area (i.e., largest decreases in permafrost stability) corresponding to climate variations. Nonetheless, the results suggest that combined impacts from three processes that increase permafrost area (i.e., two changes in soil physics and wind compaction of snow) act to strengthen the net permafrost stability. Consequently, these results imply that the incorporation of these processes in other LSMs have the potential to reduce the simulated future permafrost thaw therein, at least in the near-decadal time scales. There is however a caveat to note. For the historical conditions and time scales presented in this study, the 0–3 m soil temperatures in *NEW* (containing deep soils) is cooler than for *NEW-NO-DS* (no deep soils) at seasonal, annual to multidecadal time scales. Over longer time scales, such as till year 2100 or higher, the role of deep soils to maintain significantly higher permafrost area may be in question (e.g., as in *Lawrence et al*. [2008]). This may mostly be because of the drastic warming in projected climate toward the end of the current century, which may "overpower" the resistance from any stabilizing impacts from soil/snow physics. But this remains unresolved, as results from a coupled climate model setup are expected to be very different from using a land model setup that is forced with off-line meteorological data (such as in the study of *Lawrence et al*. [2008]).

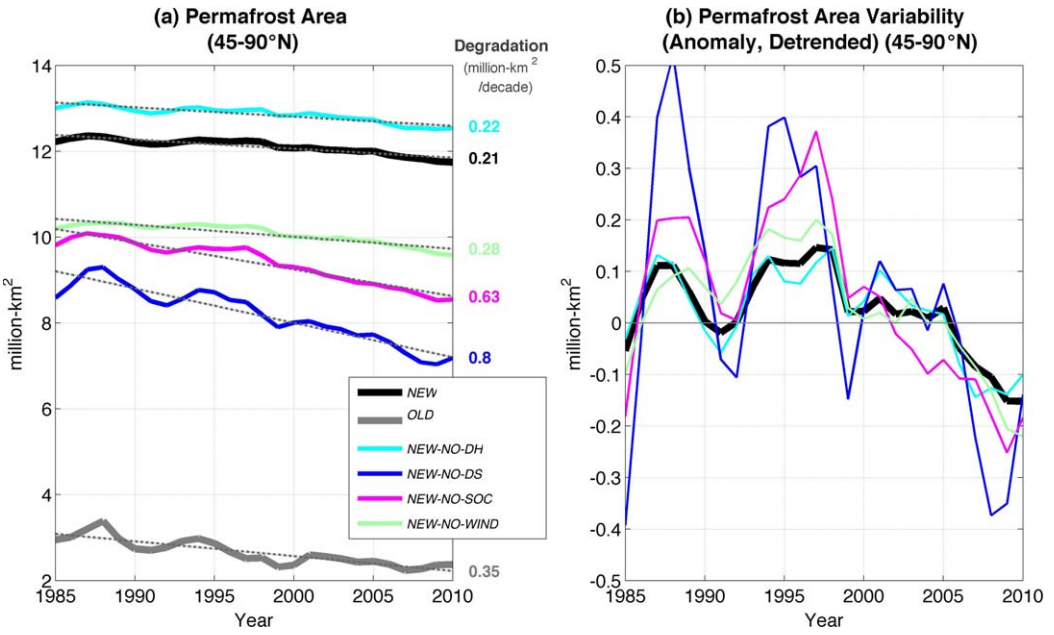

Figure 6. (a) Simulated time series and linear trends of permafrost degradation, poleward of 45°N, for *NEW*, *OLD*, and four *Interm* simulations. (b) Variability (detrended) in permafrost area time series in *NEW* and *Interm* simulations.

Similarly, the possible extent of SOC in stabilizing the 0–3 m soil temperatures at century time scales also remains less clear, as it can warm up rather quickly (by the virtue of being on the top) as well as decompose, more so with higher projected climate warming in the future.

3.1.3. Soil Temperature and Moisture

Besides the importance of the cold-region soil/snow improvements in modeling permafrost area and degradation, there are concurrent impacts on soil biogeochemistry. Permafrost area and degradation are model diagnostic properties, determined using soil temperatures within the ~0–3 m soil column. However, of primary implication for terrestrial biosphere models is that soil biogeochemical activities typically occur within the root zone (typically within 0–1 m for NHL ecosystems). Therefore, of major consequence to soil biogeochemical calculations in models are soil temperature and moisture within the shallow soil column. In this context, we find that relative contributions from the four soil/snow processes on NHL averaged soil temperature within 0–1 ($STem_{0-1m}$) is different from that in ~0–3 m (Figure 4c). As discussed previously, the inclusion of a deep soil column, SOC impacts on soil properties, and wind compaction of snow individually cools the soil, while depth hoar has a warming effect. However, the magnitude of impact from deep soil column on $STem_{0-1m}$ is minimal while wind compaction appears to play the strongest role. Such a role is further illustrated in geographical plots of individual effects of these processes on $STem_{0-1m}$ as well as root zone moisture ($SWat_{0-1m}$) (Figures 7a and 7b). As shown, the SOC-driven impacts on $STem_{0-1m}$ and $SWat_{0-1m}$ are particularly strong in the NHL permafrost-affected areas where the 0–1 m soil column is rich in organic carbon [*Tarnocai et al*., 2009]. The areas of impact due to wind compaction of snow and depth hoar are similar to that previously presented in this study for permafrost area.

Finally, the changes in soil/snow processes have very small impacts on the magnitudes of annual terrestrial energy/water fluxes in the NHL (supporting information Table S2). This implies that while the modeling improvements in soil/snow physics can be of critical importance in better simulating the permafrost physical states, it is not so for the energy/water fluxes (constrained primarily by meteorology and land-cover). Consequently, across different models, it may be less clear whether implementation of these processes will lead to improvements in the modeled energy/water fluxes with respect to observations, due to model biases from other processes, and the inherent limits of observational accuracy in flux tower data (due to systematic and random errors).

3.2. Comparison With Climate and Land-Cover Uncertainties

Due to the similar warming trends in the CRUNCEP and the NCEP (supporting information Figure S2), the simulated permafrost degradation rates are also very similar. However, the mean annual temperature in the

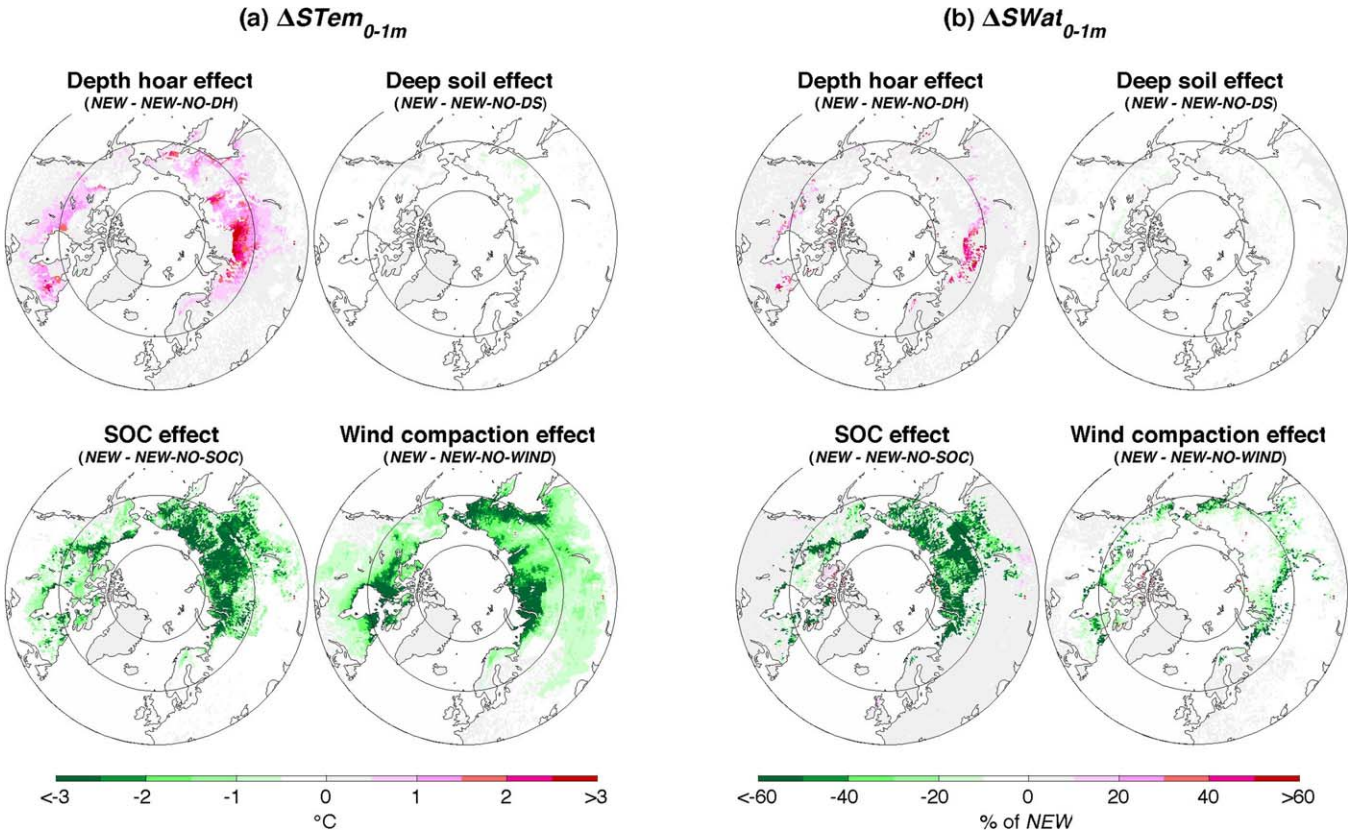

Figure 7. (a) Simulated effects on annual soil temperature in 0–1 m depth ($STem_{0-1m}$) due to individual *inclusion* of depth hoar formation, deep soils, effects of SOC on soil thermal/hydrological properties, and wind compaction of snow. (b) Corresponding effects on annual soil water in 0–1 m depth ($SWat_{0-1m}$). The results shown are for averaged period during 2000–2004.

NCEP is ~0.5°C warmer than in the CRUNCEP, and this consistently produced less permafrost in the NCEP-driven cases (Table 1). Between the two land-cover data sets (LC1 and LC2) even though there is substantial difference in boreal forest area in the NHL region (Figure 2), the corresponding differences in modeled permafrost area appear to be minimal for most cases.

To more explicitly quantify the relative contributions of differences in permafrost characteristics due to three factors considered in this study, i.e., differences/uncertainties in (1) soil/snow physics (*MODEL*), (2) climate data set (*CLIMATE*), and (3) land-cover data set (*LC*), we isolated their effects based on our series of simulations. The results (Figure 8) are based on eight simulations where *MODEL* was varied between *New* and *Old*, *CLIMATE* was varied between CRUNCEP and NCEP, and *LC* was varied between LC1 and LC2. For each factor, the statistics (boxplot) were calculated amongst simulations by varying only the respective factor, keeping everything else the same. For example, to compute *MODEL* statistics for any variable (e.g., permafrost area), differences were calculated between pairs of simulations where the climate and the land-cover data sources were identical but the physics varied between *New* and *Old* categories: (*NEW*, *OLD*), ($NEW_{CRUNCEP-LC2}$, $OLD_{CRUNCEP-LC2}$), ($NEW_{NCEP-LC1}$, $OLD_{NCEP-LC1}$), and ($NEW_{NCEP-LC2}$, $OLD_{NCEP-LC2}$). For permafrost area (Figure 8a), this shows that the combined impacts of the soil/snow improvements largely dominate over the existing climate and land-cover uncertainties, accounting for differences of up to ~8–9 $\times$ 10^6 km^2 (averaged during 2000–2004). In comparison, the climate differences produced differences of ~0.3–2.3 $\times$ 10^6 km^2, with much lower impacts from land-cover differences: ~0–0.7 $\times$ 10^6 km^2. Note that between the two reanalyses, the maximum difference in permafrost area of 2.3 $\times$ 10^6 km^2 is comparable to the contribution from individual soil/snow processes such as from wind compaction of snow, and effect of organic carbon on soil properties (Figure 4a). Given these discrepancies in historical meteorological data from two reanalyses are sufficient to produce permafrost area difference of ~2 $\times$ 10^6 km^2 in the model, larger differences using a broader range of currently available reanalyses data sets, or output from multiple ESMs can be expected to more strongly impact the permafrost characteristics for present and future time period. A

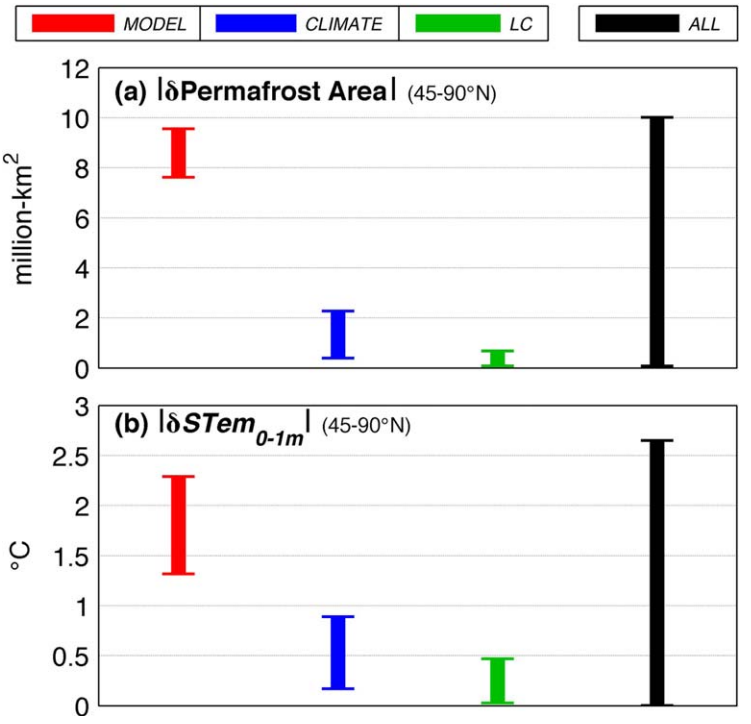

Figure 8. Attribution of modeling differences ($|\delta|$) on key permafrost physical characteristics due to differences in three factors: soil/snow parameterizations (*MODEL*), climate data sets (*CLIMATE*), and land-cover data sets (*LC*). *ALL* represents net differences due to all the factors in tandem. The variables shown are mean annual (a) permafrost area and (b) soil temperature in 0–1 m depth ($STem_{0-1m}$), using model output poleward of 45°N and averaged during 2000–2004.

similar pattern of relative importance of the three factors (*MODEL* > *CLIMATE* > *LC*) is also evident in the root zone soil temperatures ($STem_{0-1m}$; Figure 8b), though the relative influence from *CLIMATE* is slightly enhanced than for permafrost area.

3.3. Sensitivity of Results to Permafrost Threshold Temperature

For the results presented in this study, we used a temperature threshold of 0°C (monthly average) temperature to detect the presence of permafrost, which is in accordance with existing norms. However, performing further analysis of the role of the chosen threshold temperature on the diagnosed permafrost area (Figure 9) shows that permafrost area in the model is highly sensitive to the chosen temperature threshold within the range of ~−1°C to 0.25°C. Permafrost area is minimum using a −1°C threshold, and increases monotonically till a threshold of ~0.25°C. Above this, the results show negligible gains in permafrost area till the analyzed threshold of ~1°C. Note that there are large permafrost areas with soil temperature around 0°C, as the thermal inertia of the soil is enormous around the zero curtain. While this is primarily linked to soil physics, the ongoing climate change (reflected through warming in the meteorological data sets) also directly impacts the final distribution of grid cells around the zero curtain. Notably, when permafrost thaws on large scales, as is the case today, larger regions will be around the zero curtain because it takes time to melt the ice. In all simulations, the permafrost area increases most rapidly within the threshold band of −0.25°C to 0.25°C. Hence, this suggests that many model grid cells (mostly in the southern permafrost latitudes) are on the "edge" of being diagnosed as permafrost, and are most susceptible to lose the permafrost tag with small biases in meteorological/climate forcing data sets. Therefore, in multimodel intercomparison studies, small differences in the biogeophysical schemes and/or climatic forcings may lead to much larger differences in the resulting permafrost area. Given such a strong sensitivity as shown in our analysis, the permafrost extent with a fixed threshold may not be a good indicator of model performance in multimodel intercomparison projects. In future analyses, if permafrost is diagnosed as a function of threshold temperature, it may enable us to better understand the impacts of model-data shortcomings on simulated permafrost characteristics.

3.4. Limitations

We recognize several limitations in the current model and in the results. These are as follows. (1) lack of subgrid-scale parameterizations to represent sporadic and isolated permafrost types (with fractional grid cell coverage of <50%). Currently, if such areas are identified as permafrost in the model, it is most likely a result of cold soil temperature bias, due to model limitations and/or biases in input meteorology. (2) Large uncertainties in SOC data at depths below ~1 m [*Hugelius et al.*, 2014; *Mishra et al.*, 2013; *Tarnocai et al.*, 2009], as well as in modeled output [*Tian et al.*, 2015; *Todd-Brown et al.*, 2013]. Because soil physical properties in the model are constrained using data sets itself, it introduces limitations. To minimize these impacts, SOC below 1 m of soil column is constrained to zero. This is most likely to strongly impact our results in areas of deep SOC, e.g., Yedoma. Such impacts will need to be quantified in the future when uncertainties in deep SOC data are

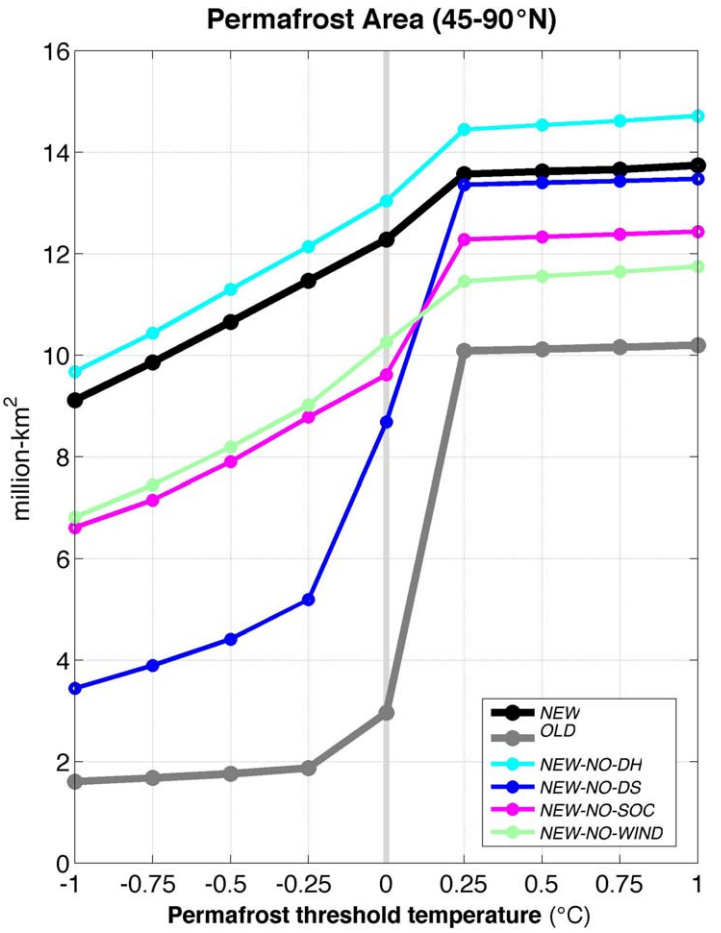

Figure 9. Sensitivity of diagnosed permafrost area in simulations to the threshold soil temperature (monthly average) to diagnose permafrost. Typically, a value of 0°C is used in existing literature.

reduced, and with corresponding improvements in the model for associated processes. (3) Use of static snow class types [*Sturm et al.*, 1995] to parameterize wind compaction and depth hoar impacts on snow. The snow class of a grid cell is prescribed during model initialization, which does not vary subsequently based on climate change over time. While this approach may not be as limiting for estimating current permafrost, the use of dynamic classes (i.e., allowing snow classes to evolve with climate regimes) may be more appropriate for projection studies. Such parameterizations do not currently exist in literature. (4) Simplified representation of thermal conductivity of depth hoar. We used constant thermal conductivities of 0.18 and 0.072 W/m/K for depth hoar in tundra and taiga regions, respectively, based on limited field observations from previous studies [*Schaefer et al.*, 2009; *Sturm and Benson*, 1997; *Sturm and Johnson*, 1992]. It is very likely that these constants are too limiting because they cannot account for variability of depth hoar properties with the same snow class. Given the importance of wind compaction and depth hoar processes as quantified here (e.g., on soil temperature and moisture), the sensitivity of these constants need further evaluation. (5) Lack of land-cover types such as peatland (bog and fen), wetland, etc. [*Lehner and Döll*, 2004]. Biogeophysical and biogeochemical processes that occur in these environments are different from soil processes; these have consequences for calculation of both permafrost physical characteristics and SOC. In the future, improvements in these aspects are expected to improve the simulated permafrost characteristics.

4. Conclusions

We show that cold-region soil/snow biogeophysics can strongly affect the simulation of NHL permafrost area, degradation, and soil thermal and hydrological states in land surface models. With respect to observations, there can be strong negative biases in the simulated permafrost area when critical soil/snow processes are excluded in the model. Much of these biases can be corrected by their inclusion. Many of these processes/parameterizations are currently missing even in the current generation of LSMs and ESMs. Therefore, as demonstrated here such models are likely to benefit by including them in their land surface schemes. Besides the modeling improvements, we discuss limitations in the model, such as the lack of subgrid variability in representing permafrost classes with less than 50% grid area coverage, limited land-cover classification types, and other factors. Necessary parameterizations for many such processes are still being developed in the community. When they are available in the future, they can be expected to further improve the permafrost physical characteristics in the model.

A specific goal of this study was to quantify the importance of each of the four soil/snow processes on permafrost physical characteristics, including soil thermal and hydrological states. In diagnosing the permafrost area and degradation (for 0–3 m soil column), the strongest contribution of deep soil thermal dynamics is evident, followed by insulating properties from SOC, wind compaction of snow, and depth hoar formation. However, the importance of these processes on soil energetics and hydrology changes with depth. Most importantly, in the soil column dominated by vegetation root zone (~0–1 m), the influence of deep soils becomes minimal. Biogeochemical activities in soils, which are primarily active within the root zone and dependent on soil temperature/moisture therein, are therefore likely to be minimally influenced by inclusion of deep soil thermal dynamics. In this context, we show that wind compaction of snow, SOC-induced modifications in soil properties and depth hoar formation—all of which are prevalent in the high-latitude environments, influence the root zone temperature/moisture to a great extent. Therefore, these can be expected to improve model estimation of permafrost SOC within the top 1 m of soil column. Note that as also shown in this study, permafrost area in the model can be highly sensitive to the threshold for soil temperature to diagnose permafrost. But, because the choice of this threshold does not affect the simulated soil states itself, the diagnosed NHL permafrost area in a model may be decoupled from the corresponding estimates of NHL SOC (i.e., more permafrost area may not imply more simulated SOC in the NHL).

Besides the contribution from soil/snow processes, we also show that climatic uncertainties in data sets can produce notable differences in NHL permafrost area (e.g., a difference of ~0.5°C in mean annual air temperatures between the two reanalyses lead to a permafrost area difference of 2.3×10^6 km^2). Given that much larger meteorological differences occur across currently available reanalysis data sets, we argue that climate-driven uncertainties are likely to play a much greater role when using these data sets. The implications of even greater differences in surface meteorology across models in multimodel intercomparison projects are therefore likely to be tremendous for permafrost area and thermal state, both for the present and for the future. This should also be true for NHL energy/water fluxes, which are influenced the least from soil/snow changes investigated here, but are majorly impacted by differences in climate and/or land-cover.

Acknowledgments

We thank David M. Lawrence, Anthony D. McGuire, and John Walsh for their comments on an earlier version of this manuscript. This work was supported in part by NASA Earth and Space Science Fellowship (NNX11AP85H) and the U.S. Department of Energy (DOE-DE-SC0006706). The data used in this paper can be accessed on request from the corresponding author R.B. (account1.rahul@gmail.com). R.B. carried out the research and wrote the paper. A.K.J. served as research advisor and provided comments. Supporting information is available in the online version of the paper. We declare no competing financial interests.

References

ACIA (2004), *Impacts of a Warming Arctic-Arctic Climate Impact Assessment*, 144 pp., Cambridge Univ. Press, Cambridge, U. K.

Anderson, E. A. (1976), A point energy and mass balance model of a snow cover, NOAA Tech. Rep. NWS 19, 150 pp., U.S. Dep. of Commer., Natl. Oceanic and Atmos. Admin., Natl. Weather Serv., Off. of Hydrol., Silver Spring, Md.

Barman, R., A. K. Jain, and M. Liang (2014a), Climate-driven uncertainties in modeling terrestrial energy and water fluxes: A site-level to global-scale analysis, *Global Change Biol.*, *20*(6), 1885–1900.

Barman, R., A. K. Jain, and M. Liang (2014b), Climate-driven uncertainties in modeling terrestrial gross primary production: A site level to global-scale analysis, *Global Change Biol.*, *20*(5), 1394–1411.

Boike, J., M. Langer, H. Lantuit, S. Muster, K. Roth, T. Sachs, P. Overduin, S. Westermann, and A. D. McGuire (2012), Permafrost–physical aspects, carbon cycling, databases and uncertainties, in *Recarbonization of the Biosphere*, edited by R. Lal, et al., pp. 159–185, Springer, Dordrecht, Netherlands.

Brown, J., O. J. Ferrians Jr., J. A. Heginbottom, and E. S. Melnikov (1997), *Circum-Arctic Map of Permafrost and Ground-Ice Conditions*, U.S. Geol. Surv., Reston, Va.

Brown, R. D., and B. Brasnett (2010), Canadian Meteorological Centre (CMC) daily snow depth analysis data, http://nsidc.org/data/docs/daac/nsidc0447_CMC_snow_depth/index.html, Natl. Snow and Ice Data Cent., Boulder, Colo.

Chadburn, S., E. Burke, R. Essery, J. Boike, M. Langer, M. Heikenfeld, P. Cox, and P. Friedlingstein (2015), An improved representation of physical permafrost dynamics in the JULES land surface model, *Geosci. Model Dev. Discuss.*, *8*(1), 715–759.

Dankers, R., E. J. Burke, and J. Price (2011), Simulation of permafrost and seasonal thaw depth in the JULES land surface scheme, *Cryosphere*, *5*(3), 773–790.

Dee, D., J. Fasullo, D. Shea, J. Walsh, and N. C. A. R. Staff (Eds). (2015), *The Climate Data Guide: Atmospheric Reanalysis: Overview & Comparison Tables*. [Available at https://climatedataguide.ucar.edu/climate-data/atmospheric-reanalysis-overview-comparison-tables, https://climatedataguide.ucar.edu/climate-data/atmospheric-reanalysis-overview-comparison-tables#sthash.A9PHMkKF.dpuf.]

Eliseev, A. V., M. M. Arzhanov, P. F. Demchenko, and I. I. Mokhov (2009), Changes in climatic characteristics of Northern Hemisphere extratropical land in the 21st century: Assessments with the IAP RAS climate model, Izvestiya, *Atmos. Oceanic Phys.*, *45*(3), 271–283.

El-Masri, B., R. Barman, P. Meiyappan, Y. Song, M. Liang, and A. K. Jain (2013), Carbon dynamics in the Amazonian Basin: Integration of eddy covariance and ecophysiological data with a land surface model, *Agric. For. Meteorol.*, *182–183*, 156–167.

Euskirchen, E. S., et al. (2006), Importance of recent shifts in soil thermal dynamics on growing season length, productivity, and carbon sequestration in terrestrial high-latitude ecosystems, *Global Change Biol.*, *12*(4), 731–750.

FAO/IIASA/ISRIC/ISS-CAS/JRC (2012), *Harmonized World Soil Database* (Version 1.10), FAO, Rome.

Fekete, B. M., C. J. Vörösmarty, and W. Grabs (1999), Global, Composite Runoff Fields Based on Observed River Discharge and Simulated Water Balances, *Tech. Rep.* 22, Global Runoff Data Cent., Koblenz, Germany.

Grosse, G., J. Harden, M. Turetsky, A. D. McGuire, P. Camill, C. Tarnocai, S. Frolking, E. A. G. Schuur, T. Jorgenson, and S. Marchenko (2011), Vulnerability of high-latitude soil organic carbon in North America to disturbance, *J. Geophys. Res.*, *116*, G00K06, doi:10.1029/2010JG001507.

Hugelius, G., J. Strauss, S. Zubrzycki, J. W. Harden, E. Schuur, C.-L. Ping, L. Schirrmeister, G. Grosse, G. J. Michaelson, and C. D. Koven (2014), Estimated stocks of circumpolar permafrost carbon with quantified uncertainty ranges and identified data gaps, *Biogeosciences*, *11*(23), 6573–6593.

Klein Goldewijk, K., A. Beusen, G. Van Drecht, and M. De Vos (2011), The HYDE 3.1 spatially explicit database of human-induced global land-use change over the past 12,000 years, *Global Ecol. Biogeogr.*, *20*(1), 73–86.

Koven, C., W. J. Riley, and A. Stern (2013), Analysis of permafrost thermal dynamics and response to climate change in the CMIP5 Earth system models, *J. Clim.*, *26*, 1877–1900.
Lawrence, D. M., and A. G. Slater (2008), Incorporating organic soil into a global climate model, *Clim. Dyn.*, *30*(2–3), 145–160.
Lawrence, D. M., A. G. Slater, V. E. Romanovsky, and D. J. Nicolsky (2008), Sensitivity of a model projection of near-surface permafrost degradation to soil column depth and representation of soil organic matter, *J. Geophys. Res.*, *113*, F02011, doi:10.1029/2007JF000883.
Lehner, B., and P. Döll (2004), Development and validation of a global database of lakes, reservoirs and wetlands, *J. Hydrol.*, *296*(1), 1–22.
Marchenko, S., V. Romanovsky, and G. Tipenko (2008), Numerical modeling of spatial permafrost dynamics in Alaska, paper presented at Ninth International Conference on Permafrost, Inst. of North. Eng., Univ. of Alaska Fairbanks, Fairbanks.
McGuire, A. D., F. S. Chapin III, J. E. Walsh, and C. Wirth (2006), Integrated regional changes in arctic climate feedbacks: Implications for the global climate system, *Annu. Rev. Environ. Resour.*, *31*, 61–91.
Meiyappan, P., and A. K. Jain (2012), Three distinct global estimates of historical land-cover change and land-use conversions for over 200 years, *Frontiers Earth Sci.*, *6*(2), 122–139.
Mishra, U., J. D. Jastrow, R. Matamala, G. Hugelius, C. D. Koven, J. W. Harden, C. L. Ping, G. J. Michaelson, Z. Fan, and R. M. Miller (2013), Empirical estimates to reduce modeling uncertainties of soil organic carbon in permafrost regions: A review of recent progress and remaining challenges, *Environ. Res. Lett.*, *8*(3), 035020.
Qian, T., A. Dai, K. E. Trenberth, and K. W. Oleson (2006), Simulation of global land surface conditions from 1948 to 2004. Part I: Forcing data and evaluations, *J. Hydrometeorol.*, *7*(5), 953–975.
Saito, K., M. Kimoto, T. Zhang, K. Takata, and S. Emori (2007), Evaluating a high-resolution climate model: Simulated hydrothermal regimes in frozen ground regions and their change under the global warming scenario, *J. Geophys. Res.*, *112*, F02S11, doi:10.1029/2006JF000577.
Schaefer, K., T. Zhang, A. G. Slater, L. Lu, A. Etringer, and I. Baker (2009), Improving simulated soil temperatures and soil freeze/thaw at high-latitude regions in the Simple Biosphere/Carnegie-Ames-Stanford Approach model, *J. Geophys. Res.*, *114*, F02021, doi:10.1029/2008JF001125.
Schaefer, K., T. Zhang, L. Bruhwiler, and A. P. Barrett (2011), Amount and timing of permafrost carbon release in response to climate warming, *Tellus, Ser. B*, *63*(2), 165–180.
Schuur, E., et al. (2012), Expert assessment of vulnerability of permafrost carbon to climate change, *Clim. Change*, *119*, 359–374.
Schuur, E., A. D. McGuire, C. Schädel, G. Grosse, J. W. Harden, D. J. Hayes, G. Hugelius, C. D. Koven, P. Kuhry, and D. M. Lawrence (2015), Climate change and the permafrost carbon feedback, *Nature*, *520*(7546), 171–179.
Sellers, P. J., D. A. Randall, G. J. Collatz, J. A. Berry, C. B. Field, D. A. Dazlich, C. Zhang, G. D. Collelo, and L. Bounoua (1996), A revised land surface parameterization (SiB2) for atmospheric GCMs. Part I: Model formulation, *J. Clim.*, *9*(4), 676–705.
Slater, A. G., and D. M. Lawrence (2013), Diagnosing present and future permafrost from climate models, *J. Clim.*, *26*, 5608–5623.
Sturm, M., and C. S. Benson (1997), Vapor transport, grain growth and depth-hoar development in the subarctic snow, *J. Glaciol.*, *43*(143), 42–59.
Sturm, M., and J. B. Johnson (1992), Thermal conductivity measurements of depth hoar, *J. Geophys. Res.*, *97*(B2), 2129–2139.
Sturm, M., J. Holmgren, and G. E. Liston (1995), A seasonal snow cover classification system for local to global applications, *J. Clim.*, *8*, 1261–1283.
Tarnocai, C., J. G. Canadell, E. A. G. Schuur, P. Kuhry, G. Mazhitova, and S. Zimov (2009), Soil organic carbon pools in the northern circumpolar permafrost region, *Global Biogeochem. Cycles*, *23*, GB2023, doi:10.1029/2008GB003327.
Tian, H., et al. (2015), Global patterns and controls of soil organic carbon dynamics as simulated by multiple terrestrial biosphere models: Current status and future directions, *Global Biogeochem. Cycles*, *29*, 775–792, doi:10.1002/2014GB005021.
Todd-Brown, K. E., J. T. Randerson, W. M. Post, F. M. Hoffman, C. Tarnocai, E. A. Schuur, and S. D. Allison (2013), Causes of variation in soil carbon simulations from CMIP5 Earth system models and comparison with observations, *Biogeosciences*, *10*(3), 1717–1736.
Viovy, N., and P. Ciais (2011), *CRUNCEP data set for 1901–2008, Tech. Rep. Version 4*, Laboratoire des Sciences du Climat etde l'Environnement. [Available at http://dods.extra.cea.fr/data/p529viov/cruncep/, accessed September 2012.]
Wei, Y., S. Liu, D. N. Huntzinger, A. M. Michalak, N. Viovy, W. M. Post, C. R. Schwalm, K. Schaefer, A. R. Jacobson, and C. Lu (2013), The North American carbon program multi-scale synthesis and terrestrial model intercomparison project—Part 2: Environmental driver data, *Geosci. Model Dev. Discuss.*, *6*(4), 5375–5422.
Yang, X., V. Wittig, A. K. Jain, and W. Post (2009), Integration of nitrogen cycle dynamics into the Integrated Science Assessment Model for the study of terrestrial ecosystem responses to global change, *Global Biogeochem. Cycles*, *23*, GB4029, doi:10.1029/2009GB003474.
Zhang, T., T. E. Osterkamp, and K. Stamnes (1996), Influence of the depth hoar layer of the seasonal snow cover on the ground thermal regime, *Water Resour. Res.*, *32*(7), 2075–2086.
Zhang, T., R. G. Barry, K. Knowles, J. A. Heginbottom, and J. Brown (1999), Statistics and characteristics of permafrost and ground-ice distribution in the Northern Hemisphere 1, *Polar Geogr.*, *23*(2), 132–154.